ELSEVIER

Ceramics International 33 (2007) 843–849

CERAMICS INTERNATIONAL

www.elsevier.com/locate/ceramint

Structure and colour of cobalt ceramic pigments from phosphates

S. Meseguer, M.A. Tena *, C. Gargori, J.A. Badenes, M. Llusar, G. Monrós

Inorganic Chemistry Area, Inorganic and Organic Chemistry Department, Jaume I University, Castellón, Spain

Received 10 November 2005; received in revised form 22 December 2005; accepted 3 January 2006
Available online 27 April 2006

Abstract

$Co_{3-x}Fe_xP_2O_{8+x/2}$ ($0 \leq x \leq 2.0$) and $Fe_{1-x}Co_xPO_{4-x/2}$ ($0 \leq x \leq 0.5$) compositions were synthetized by the chemical coprecipitation method and characterized by differential thermal analysis and thermogravimetric analysis, X-ray diffraction, UV–vis–NIR spectroscopy, CIE L^* a^* b^* parameters measurements and electronic microscopy. At 1000 °C, $Co_3(PO_4)_2$ solid solutions ($Co_{3-x}Fe_xP_2O_{8+x/2}$; $0 \leq x \leq 0.3$) and $FePO_4$ solid solutions ($Fe_{1-x}Co_xPO_{4-x/2}$; $0 \leq x \leq 0.02$) were obtained. From enamelled samples, the blue colouration is detected when an appreciable amount of $Co_3(PO_4)_2$ ($Co_{3-x}Fe_xP_2O_{8+x/2}$ samples) or $Co_2P_2O_7$ ($Fe_{1-x}Co_xPO_{4-x/2}$ samples) is present in powdered samples. These materials develop blue colourations in enamelled samples when $0 \leq x \leq 1.0$ in $Co_{3-x}Fe_xP_2O_{8+x/2}$ (between 48 and 32 wt.% Co) compositions and when $x \geq 0.30$ in $Fe_{1-x}Co_xPO_{4-x/2}$ (≥12 wt.% Co) compositions. $Fe_{1-x}Co_xPO_{4-x/2}$ ($0.3 \leq x \leq 0.5$) compositions can be considered to minimize the Co content in blue ceramic pigments.

Keywords: B. Spectroscopy; C. Colour; D. Traditional ceramics

1. Introduction

Phosphates have great capacity to form solid solutions and to accept substitutes [1–5]. Modifications of the physical properties of solid solutions can be associated with the dopant cations and with changes in structure in compounds. Solid solutions of metal phosphate are used in catalytic applications [1]. Thorium-uranium (IV) phosphate-diphosphate solid solutions were studied to stabilize radionuclides in solids [2]. Eu^{3+} luminescence in doped oxyphosphate-silicate apatite was related with three distinct sites of Eu^{3+} cations in $Ca_5La_5(SiO_4)_3(PO_4)_3O_2$:Eu(2%) [3].

There are two ceramic pigments with phosphate structure in the DCMA classification [6]. They are Cobalt violet phosphate (8-11-1 DCMA) and Cobalt lithium violet phosphate (8-12-1 DCMA). The traditional source of blue in ceramic pigments is the cobalt ion [7], except for vanadium-zircon Turkish Blue (14-42-2 DCMA). The Co_2SiO_4 olivine (5-08-2 DCMA), $(Co,Zn)_2SiO_4$ willemite (7-10-2 DCMA), $CoAl_2O_4$ spinel (13-26-2 DCMA), Co_2SnO_4 (13-27-2 DCMA), $(Co,Zn)Al_2O_4$ (13-28-2 DCMA) and $Co(Al,Cr)_2O_4$ (13-28-2 DCMA) are further blue pigments. All of them are widely used in the ceramic industry.

The colouring performance of cobalt pigments depends very much on their thermal stability, on their chemical reactivity towards the glaze components, and also on the coordination of Co^{2+} ions (tetrahedral coordination is preferred to octahedral). The blue colour of enamelled samples was always attributed to tetrahedrally coordinated Co^{2+} ions [8].

In a previous study, Co_2SiO_4, Co-doped willemite and a magnesium-doped Co-Al spinel reacted with the ceramic glazes selected (representative of double firing, single firing and porcelainized stoneware industrial sectors), diffusing Co^{2+} ions from their coordination sites in the pigment to be preferentially accommodated in tetrahedral sites of the glassy matrix [9].

The ceramic pigments industry tends towards cheap and simple processing. The synthesis from mixtures of solid starting materials is habitual. The necessary high temperatures give rise to loss of volatile reagents and consequently to deviation of the stoichiometric conditions of the initial systems.

Aqueous precipitation route [10] and hydrothermal synthesis [11] are commonly used methods in synthesis of phosphates. In cobalt ceramic pigments the synthesis temperature can be reduced by the use of cobalt phosphates. From $NH_4H_2PO_4$ and $CoCO_3$ mixtures, crystallization of $Co_3(PO_4)_2$ occurs at about 625 °C [12]. Temperature to obtain olivine,

* Corresponding author. Tel.: +34 964728249; fax: +34 964728214.
E-mail address: tena@qio.uji.es (M.A. Tena).

0272-8842/$32.00
doi:10.1016/j.ceramint.2006.01.024

willemite or spinel is about 1300 °C. The $Co_3(PO_4)_2$ structure is formed by distorted trigonal bipyramids CoO_5, fairly regular CoO_6 octahedra and almost regular PO_4 tetrahedra [13]. At normal pressures iron phosphate ($FePO_4$) adopts a verlinite ($AlPO_4$) structure related to α-quartz with each iron and phosphorus atom tetrahedrally bonded to four oxygen atoms. $FePO_4$ presents an α-β phase transition from a $P6_222$ to a $P3_121$ phase at 705 °C [14].

The aim of this study is the formation of $Co_{3-x}Fe_xP_2O_{8+x/2}$ and $Fe_{1-x}Co_xPO_{4-x/2}$ solid solutions to minimize the Co content of the pigment and to establish the compositional range of these solid solutions for which the materials develop blue colourations in enamelled samples.

2. Experimental procedures

$Co_{3-x}Fe_xP_2O_{8+x/2}$ $(0 \leq x \leq 2.0)$ and $Fe_{1-x}Co_xPO_{4-x/2}$ $(0 \leq x \leq 0.5)$ compositions were prepared by the chemical coprecipitation method. The starting materials were $Co(NO_3)_2$ $6H_2O$ (Merck), $Fe(NO_3)_3$ $9H_2O$ (Merck), and H_3PO_4 (Panreac) of reagent grade chemical quality. To a 0.67 M solution of H_3PO_4 in water was added an 0.67 M aqueous solution of $Co(NO_3)_2$ and/or $Fe(NO_3)_3$ with vigorous stirring at room temperature. The molar ratio was (Co + Fe)/P = 3/2 in $Co_{3-x}Fe_xP_2O_{8+x/2}$ samples and (Co + Fe)/P = 1/1 in $Fe_{1-x}Co_xPO_{4-x/2}$ samples. After that, a solution of ammonium hydroxide was added dropwise until pH 7–8. From $Co_{3-x}Fe_xP_2O_{8+x/2}$ samples, a precipitate was obtained. From $Fe_{1-x}Co_xPO_{4-x/2}$ compositions, gelation occurred with the same procedure. Finally, the precipitate or gel was dried by an infrared lamp.

Differential thermal analysis (DTA) and thermogravimetric analysis (TG) were carried out in a Mettler Toledo instrument in a synthetic air atmosphere using alumina crucible and a heating rate of 5 °C/min. From results obtained with DTA and TG, thermal treatment was designed and all the dried samples were fired in refractory crucibles at 800 and 1000 °C for 2 h of soaking times at each temperature.

The resulting materials were examined with a Siemens D5000 X-ray diffractometer to study the development of the crystalline phases at different temperatures. Unit cell parameters of $Co_3(PO_4)_2$ and $FePO_4$ were measured using LSQC and POWCAL programmes [15]. In order to refine "d" values, α-Al_2O_3 was employed as an internal standard in an X-ray diffractogramme running between 10° and 80° (2θ) at low goniometer speed. The POWCAL and LSQC programmes calculate the crystallographic unit cell parameters of the sample by comparing its refined "d" values with the standard values.

In order to test their efficiency as blue ceramic pigment, the fired compositions were 5% weight enamelled with a transparent glaze (single-firing glaze of composition 0.106 mol K_2O, 0.565 mol CaO, 0.329 mol ZnO, 0.323 mol Al_2O_3, 1.972 mol SiO_2) onto commercial ceramic biscuits. Glazed tiles were fired for 5 min at 1085 °C for the single-firing glaze in a cycle of 60 min (cold-to-cold). The properties as ceramic pigments for porcelain stoneware were also analysed. Thus, the samples were 3% weight mixed in bulk with porcelain stoneware body (spray-dried powder) and fired for 5 min at 1200 °C in a single-firing cycle of 57 min (cold-to-cold).

UV–vis spectroscopy (diffuse reflectance) allows the Co(II) site in the materials to be studied. A Lambda 2000 Perkin-Elmer spectrophotometer was used to obtain the UV–vis–NIR (ultraviolet-visible-near infrared) spectra in the 200–2000 nm range. CIE L^* a^* b^* colour parameter measurements, conducted with a Perkin-Elmer colorimeter using a standard illuminant D, were used to differentiate the samples in terms of colour. L^* is the lightness axis (black (0) −> white (1 0 0)), a^* is the green (−) −> red (+) axis, and b^* is the blue (−) −> yellow (+) axis [16]. The measurements were made on glazed tiles with addition of 5 wt.% samples fired.

Microstructural observations and microanalysis of fired samples were carried out in a scanning electron microscope, LEO 440. The surface of these specimens was previously carbon coated by sputtering.

3. Results and discussion

DTA and TG curves of $Co_3(PO_4)_2$ and $FePO_4$ samples are shown in Fig. 1. The DTA curve of $Co_3(PO_4)_2$ sample exhibits an endothermic peak about 200 °C attributed to NH_4NO_3 decomposition and loss of H_2O. In the same temperature range,

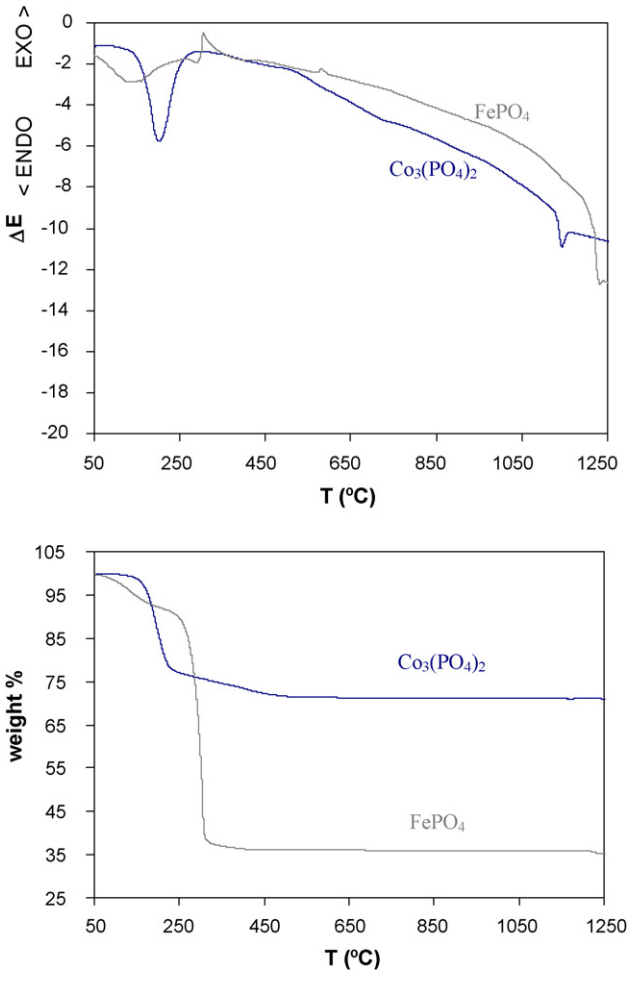

Fig. 1. ATD and TG curves of $Co_3(PO_4)_2$ and $FePO_4$.

Table 1
Crystalline phase evolution with temperature and chromatic coordinates (CIE $L^*/a^*/b^*$) in $Co_{3-x}Fe_xP_2O_{8+x/2}$ samples

x	25 °C	800 °C	1000 °C
0.00	H(m), N(m) 65.48/14.99/−13.43	C(s) 51.01/8.26/−13.91	C(s) 44.46/13.46/−17.36
0.10	H(m), N(m) 64.73/8.18/−2.67	C(s) 51.00/7.05/−7.62	C(s) 45.15/10.78/−10.35
0.30	H(m), N(m) 63.83/4.28/0.41	C(s) 50.78/6.10/0.68	C(s) 44.12/8.33/−0.34
0.50	H(m), N(m), O(w) 60.11/3.48/−2.25	C(s), F(vw) 42.04/0.51/1.28	C(s), F(w) 39.96/0.22/0.33
0.70	N(m) 62.47/3.3/−5.27	C(s), OP(m) 47.61/4.59/7.5	C(s), OP(m) 41.96/4.82/3.74
1.00	N(m) 57.64/6.75/−1.01	C(m), OP(m), P(w) 45.37/3.57/6.96	C(m), OP(m), P(m) 41.91/4.09/4.37
1.50	N(m) 60.07/4.63/9.61	P(m), OP(m) 44.61/1.35/7.6	P(m), OP(m) 44.13/0.22/6.34
2.00	N(m) 55.36/8.4/16.86	OP(m), C(vw) 39.76/0.24/1.38	OP(m), C (vw) 41.78/2.45/5.05

Crystalline phases: H = $Co_3(PO_4)_2{\cdot}8H_2O$, C = $Co_3(PO_4)_2$, O = $Fe_2PO_4(OH)$, F = γ-Fe_2O_3, N = NH_4NO_3, OP = $CoFeO(PO_4)$, P = $Co_3\ Fe_4(PO_4)_6$. Diffraction peak intensity: s = strong, m = medium, w = weak, vw = very weak.

a weight decrease is detected in the TG curve. A slight loss of weight is observed until 450 °C in this sample. Endothermic peaks at 100–300 °C in DTA curve of $FePO_4$ sample and a great loss of weight in the same temperature range in TG curve of this sample are associated with the evaporation of residual solvent entrapped in the micropores of gel and NH_4NO_3 decomposition. Endothermic peaks at 1148 and 1240 °C in DTA curves are assigned to $Co_3(PO_4)_2$ and $FePO_4$ melting, respectively [12,14]. No noticeable changes are observed from TG curves at 500–1100 °C temperature range.

The variation of crystalline phases with temperature and the CIE L^*, a^* and b^* parameters in fired samples are shown in Tables 1 and 2. When (Co + Fe)/P molar ratio was 3/2 ($Co_{3-3x/2}Fe_xP_2O_{8+x/2}$ samples) and $0 \leq x \leq 0.3$, $Co_3(PO_4)_2$ is the only phase obtained at 800 and 1000 °C. In these samples, γ-Fe_2O_3, $CoFeO(PO_4)$ or $Co_3Fe_4(PO_4)_6$ are also detected when $x > 0.3$. In $Fe_{1-x}Co_xPO_{4-x/2}$ samples ((Co + Fe)/P molar ratio of 1/1) $Co_2P_2O_7$ is detected together with $FePO_4$ crystalline phase when $x > 0.02$. From the variation of CIE L^*, a^* and b^* parameters of powdered samples, $Co_{3-3x/2}Fe_xP_2O_{8+x/2}$ compositions with $x \leq 0.10$ and the $Fe_{1-x}Co_xPO_{4-x/2}$ composition with $x = 1.00$ ($Co_2P_2O_7$) are potentially suitable for violet or blue materials ($b^*(-)$). It is related with the crystalline phase evolution. $Co_{3-3x/2}Fe_xP_2O_{8+x/2}$ compositions are violet when $0 \leq x \leq 0.30$ ($Co_3(PO_4)_2$ is detected by XRD) and these compositions are blue-black or brown when $x \geq 0.30$, according with the presence of γ-Fe_2O_3 (black) or $CoFeO(PO_4)$ (brown) in samples. Yellow and green materials are obtained from $Fe_{1-x}Co_xPO_{4-x/2}$ when $0 \leq x \leq 0.50$, according with the presence of $FePO_4$ (yellow) and $Co_2P_2O_7$ (blue).

Figs. 2 and 3 show the unit cell parameters obtained for samples fired at 1000 °C. The variation of these parameters with composition confirms the formation of the $Co_3(PO_4)_2$ solid solutions and $FePO_4$ solid solutions. In $Co_{3-3x/2}Fe_xP_2O_{8+x/2}$ samples (Fig. 2), a and c parameters decrease according with the replacement of Co^{2+} ion by a smaller one (Fe^{3+}). The variation of the b parameter with x can be attributed to structural distortion [17]. In $Fe_{1-x}Co_xPO_{4-x/2}$ samples (Fig. 3), the replacement of Fe^{3+} ion by a greater one (Co^{2+}) is in accordance with the increase of the a parameter. In these samples, the c parameter decrease with x. It can be related with changes in distances M–M and M–O (M = Fe, Co) [18]. From these results, it is possible to establish the compositional range for which the $Co_3(PO_4)_2$ or $FePO_4$ structure is maintained at 1000 °C. At this temperature, it is $0 \leq x \leq 0.30$ in $Co_{3-x}Fe_xP_2O_{8+x/2}$ samples and it is $0 \leq x \leq 0.02$ in $Fe_{1-x}Co_xPO_{4-x/2}$ samples.

Fig. 4 shows the UV–vis–NIR spectra in $Co_{3-x}Fe_xP_2O_{8+x/2}$ samples fired at 1000 °C. When $0 \leq x \leq 0.3$, the $Co_3(PO_4)_2$ is the only crystalline phase detected in these fired samples and five absorption bands are observed. These bands at 1689, 1078, 887, 582 and 495 nm are assigned to Co^{2+} in both octahedral (1078 and 582 nm) and trigonal bipyramidal (1689, 887 and 495 nm) sites. They are the two different crystallographic sites for the cobalt ion in the structure of $Co_3(PO_4)_2$ [13]. In six coordinate Co(II) complexes (high spin) a band near 1240–1000 nm can be assigned to the $^4T_{1g} \rightarrow {}^4T_{2g}$ transition. In addition a multiple structured band, assigned to $^4T_{1g} \rightarrow {}^4T_{1g}(P)$, is seen in the visible region near 500 nm. The multiple structure arises primarily from admixture of spin forbidden transitions to doublet states mainly

Table 2
Crystalline phase evolution with temperature and chromatic coordinates (CIE $L^*/a^*/b^*$) in $Fe_{1-x}Co_xPO_{4-x/2}$ samples

x	25 °C	800 °C	1000 °C
0.00	N(m) 58.64/11.92/25.14	F(s) 76.31/3.32/15.23	F(s) 69.6/5.59/18.33
0.01	N(m) 62.5/8.89/25.31	F(s) 69.47/4.98/16.68	F(s) 66.45/−1.00/13.18
0.02	N(m) 66.17/6.32/25.22	F(s) 70.01/−4.01/13.61	F(s) 64.87/−5.87/11.22
0.05	N(m) 62.63/5.04/21.59	F(s), Co(vw) 70.73/−6.38/14.12	F(s), Co(vw) 63.65/−6.83/14.18
0.10	N(m) 60.68/3.64/19.69	F(s), Co(vw) 67.18/−5.82/11.46	F(s), Co(vw) 57/−5.43/8.81
0.30	N(m) 54.16/−1.25/2.84	F(s), Co(w) 66.95/−4.8/6.7	F(s), Co(w) 59.63/−3.09/2.51
0.50	N(m) 65.95/−1.32/−4.7	F(s), Co(m) 64.93/−5.12/9.39	F(m), Co(m) 59.13/−3.7/4.48
1.00	N(w) 53.43/32.43/−28.98	Co(s) 64.19/2.11/−12.55	Co(s) 52.85/6.4/−10.38

Crystalline phases: F = $FePO_4$, Co = $Co_2P_2O_7$, N = NH_4NO_3. Diffraction peak intensity: s = strong, m = medium, w = weak, vw = very weak.

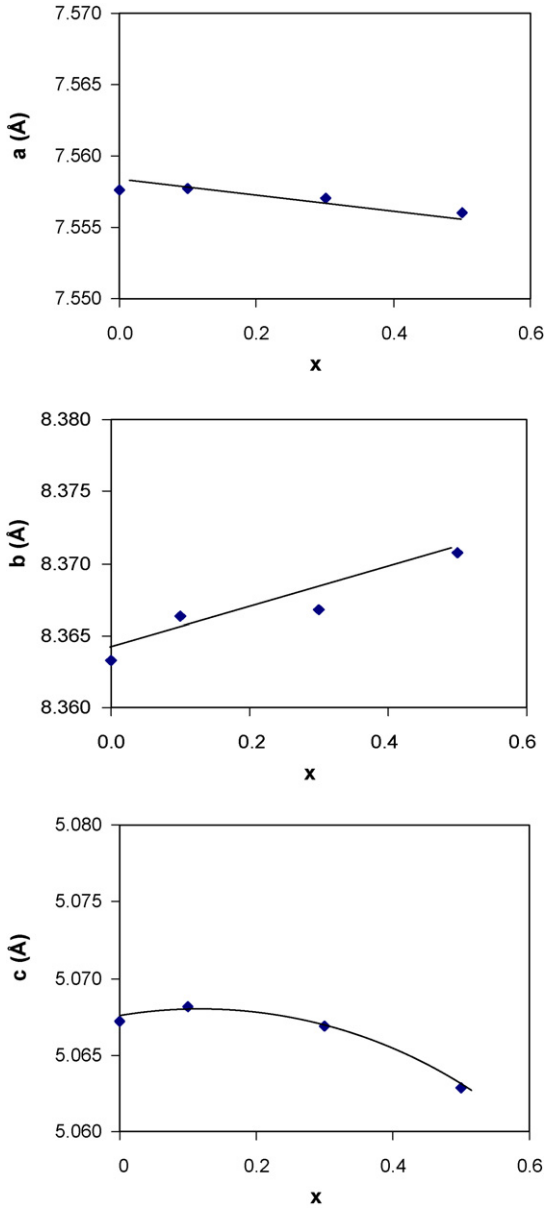

Fig. 2. Unit cell parameters in $Co_{3-x}Fe_xP_2O_{8+x/2}$ samples fired at 1000 °C.

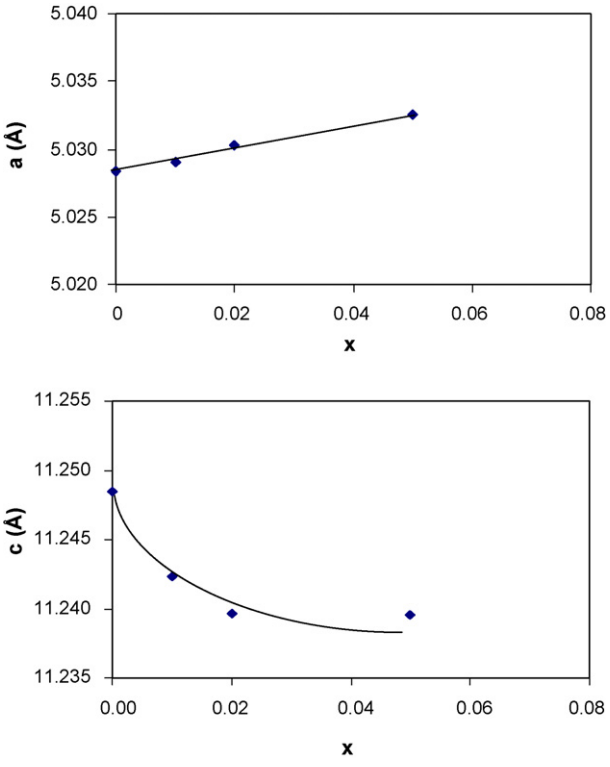

Fig. 3. Unit cell parameters in $Fe_{1-x}Co_xPO_{4-x/2}$ samples fired at 1000 °C.

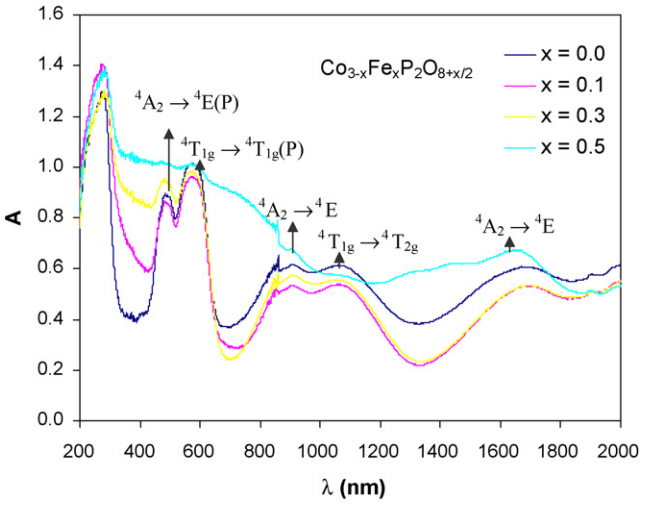

Fig. 4. UV–vis spectra of $Co_{3-x}Fe_xP_2O_{8+x/2}$ samples fired at 1000 °C.

derived from ^2G and ^2H. The transition to $^4A_{2g}$ is very weak often appearing as a shoulder. A weak feature in the spectrum near 822 nm might be the $^4A_{2g}$ transition. In high spin trigonal bipyramidal Co^{2+} sites, transitions from the $^4A_2$' ground state generally occur both in the near infrared, and in the visible region. Indeed the spectra of these species are quite rich: $^4A_2 \rightarrow {}^4A_1$, $^4A_2$ (2500–1111 nm); $^4A_2 \rightarrow {}^4E$ (1923–1724 nm); $^4A_2 \rightarrow {}^4E$ (1000–676 nm); $^4A_2 \rightarrow {}^4A_2(P)$ (752–585 nm); $^4A_2 \rightarrow {}^4E(P)$ (582–476 nm) [19]. From $x = 0.5$ sample, the change in shape of curve in Fig. 4 is related to the mixture of $Co_3(PO_4)_2$ and γ-Fe_2O_3 crystalline phases. In this sample, the observed absorption in 1230–1540, 650–820, 350–445 nm wavelength ranges is attributed to iron ion in maghemite (γ-Fe_2O_3), detected by XRD.

Fig. 5 shows the UV–vis spectra of $Co_3(PO_4)_2$ and $Co_2P_2O_7$ compounds fired at 1000 °C. Co(II) in octahedral site and Co(II) trigonal bipyramidal site are present in these structures [13,20]. Absorption bands of octahedral site in $Co_2P_2O_7$ are

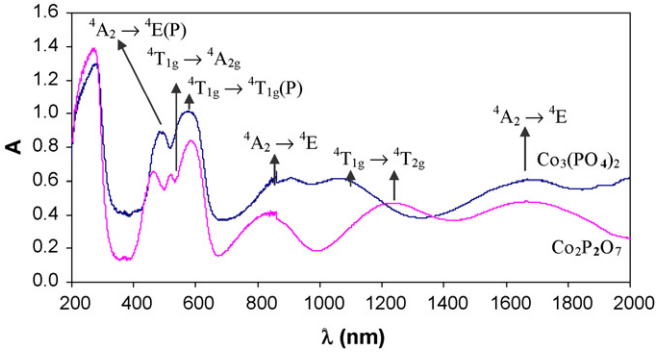

Fig. 5. UV–vis spectra of $Co_3(PO_4)_2$ and $Co_2P_2O_7$ fired at 1000 °C.

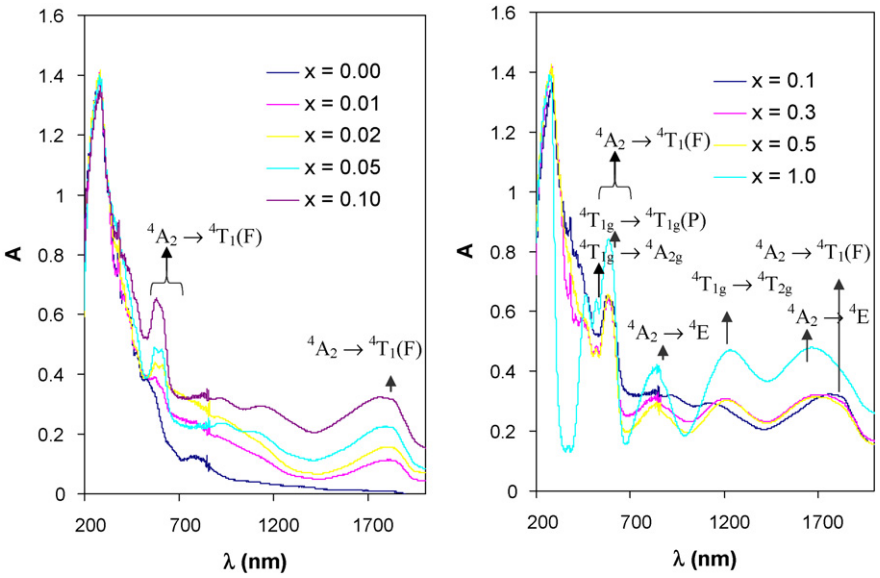

Fig. 6. UV–vis spectra of $Fe_{1-x}Co_xPO_{4-x/2}$ samples fired at 1000 °C.

observed about 1244, 592 and 525 nm. The last one is weak and it can be assigned to the transition to $^4A_{2g}$. The smaller wavelength of transitions bands in $Co_2P_2O_7$ compared with $Co_3(PO_4)_2$ (1078 and 582 nm) might be explained by the changes on crystal field strength (smaller mean Co–O distances in $Co_2P_2O_7$ compared with $Co_3(PO_4)_2$).

Fig. 6 shows the UV–vis spectra in $Fe_{1-x}Co_xPO_{4-x/2}$ samples with $0 \leq x \leq 1.0$ and fired at 1000 °C. When $x \leq 0.02$, three absorption bands are observed. These bands at 1820 and a double band with maximal absorption at 617 and 582 nm are assigned to Co^{2+} in a tetrahedral site. In four coordinate tetrahedral and pseudotetrahedral cobalt(II), the $^4A_2 \rightarrow {}^4T_1(F)$ (3333–1000 nm) and $^4A_2 \rightarrow {}^4T_1(P)$ (555–769 nm) transitions appear as multiple absorption in the near infrared and visible regions, respectively. The intensities of these bands allow a distinction to be made between tetrahedral and octahedral cobalt(II) derivates [19]. Fe^{3+} with tetrahedral coordination in $FePO_4$ structure shows weak absorption bands in visible region ($Fe_{1-x}Co_xPO_{4-x/2}$ $x = 0.0$ sample). When $x > 0.02$ bands at 1708–1750, 1160–1235, 834–841 and 586–597 nm are assigned to Co^{2+} in both octahedral and trigonal bipyramidal sites. It is in accordance with $Co_2P_2O_7$ detected by XRD.

The colour parameters (L^* a^* b^*) of enamelled samples are different from those obtained for powdered samples. The CIE L^* a^* b^* parameters in glazed tiles from samples fired at 1000 °C can be seen in Tables 3 and 4. From these results, it is possible to establish the compositional range for which the suitable blue colour is maintained in enamelled samples. It is $0 \leq x \leq 1.0$ in $Co_{3-x}Fe_xP_2O_{8+x/2}$ compositions (between 48 and 32 wt.% Co) and it is $x \geq 0.30$ in Co-$FePO_4$ compositions (about 12 wt.% Co). Nominal Co wt.% in $Fe_{0.7}Co_{0.3}PO_{3.85}$ and $Fe_{0.5}Co_{0.5}PO_{3.75}$ compositions (12 or 20%) is smaller than nominal composition in Co_2SiO_4 (56.1%) or $Co_{0.8}Mg_{0.2}Al_2O_4$ (27.7%) and the enamelled samples develop a suitable blue colour in the three cases (Tables 3 and 4). $Fe_{1-x}Co_xPO_{4-x/2}$

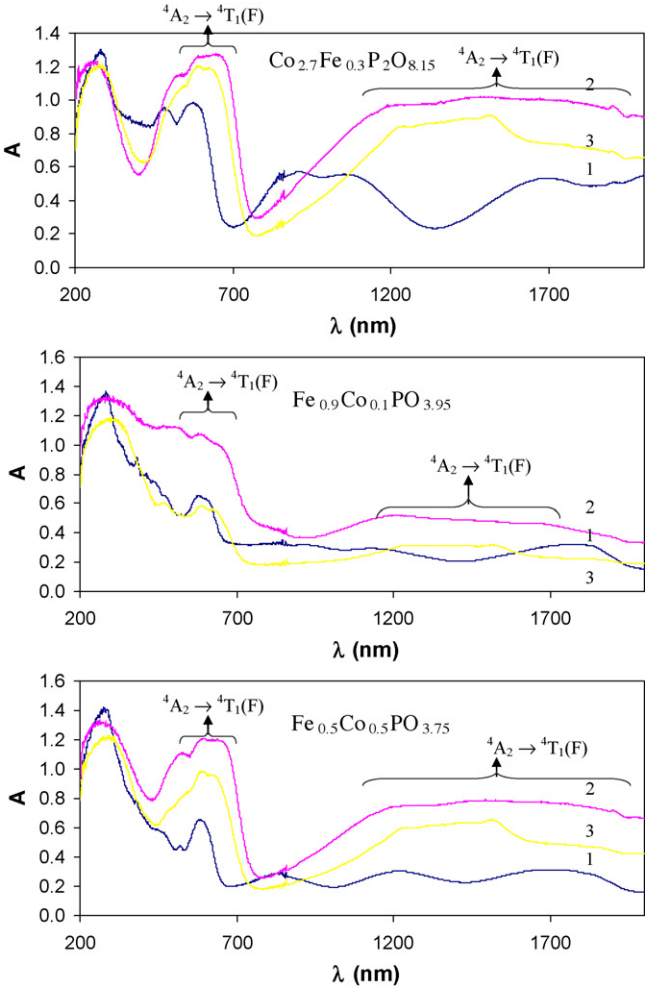

Fig. 7. UV–vis spectra of $Co_{2.7}Fe_{0.3}P_2O_{8.15}$, $Fe_{0.9}Co_{0.1}PO_{3.95}$ and $Fe_{0.5}Co_{0.5}PO_{3.75}$ samples: (1) powdered samples fired at 1000 °C, (2) enamelled samples with a single-firing glaze and (3) from porcelain stoneware.

compositions with $x \geq 0.30$ can be considered to minimize the Co content in blue ceramic pigments.

Pinhole defect is obtained from enamelled samples when cobalt amount is high (compositions close to $Co_3(PO_4)_2$ and $Co_2P_2O_7$).

UV–vis curves indicate a change in Co^{2+} coordination from 5 and 6 (powdered samples) to 4 (enamelled samples) in all prepared $Co_{3-x}Fe_xP_2O_{8+x/2}$ samples and $Fe_{1-x}Co_xPO_{4-x/2}$ samples with $x \geq 0.02$. It is in accordance with diffusing Co^{2+} ions from their coordination sites in the pigment ($Co_3(PO_4)_2$ and $Co_2P_2O_7$ structures) to tetrahedral sites of the glassy matrix. Fig. 7 shows the UV–vis spectra of $Co_{2.7}Fe_{0.3}P_2O_{8.15}$, $Fe_{0.9}Co_{0.1}PO_{3.95}$ and $Fe_{0.5}Co_{0.5}PO_{3.75}$ compositions as representative samples.

SEM/EDX analyses on powdered samples show aggregate of particles with homogeneous or heterogeneous compositions according with XRD results. From enamelled samples with transparent glaze or with porcelain stoneware different results are obtained. From transparent glaze, EDX mapping and spectra show association of Ca and P surrounding (Co,Fe)-rich region. From porcelain stoneware samples an association of Fe, Co and Zn are detected. P is homogeneous distributed in these samples. Fig. 8 shows the different distribution of P and Co in representative enamelled samples. These results confirmed that the $Co_3(PO_4)_2$ and $Co_2P_2O_7$ structures are dissolved. These structures introduce the Co^{2+} ions into glassy matrix. These ions remain in enamelled samples and the blue colour of enamelled samples is attributed to Co^{2+} ions.

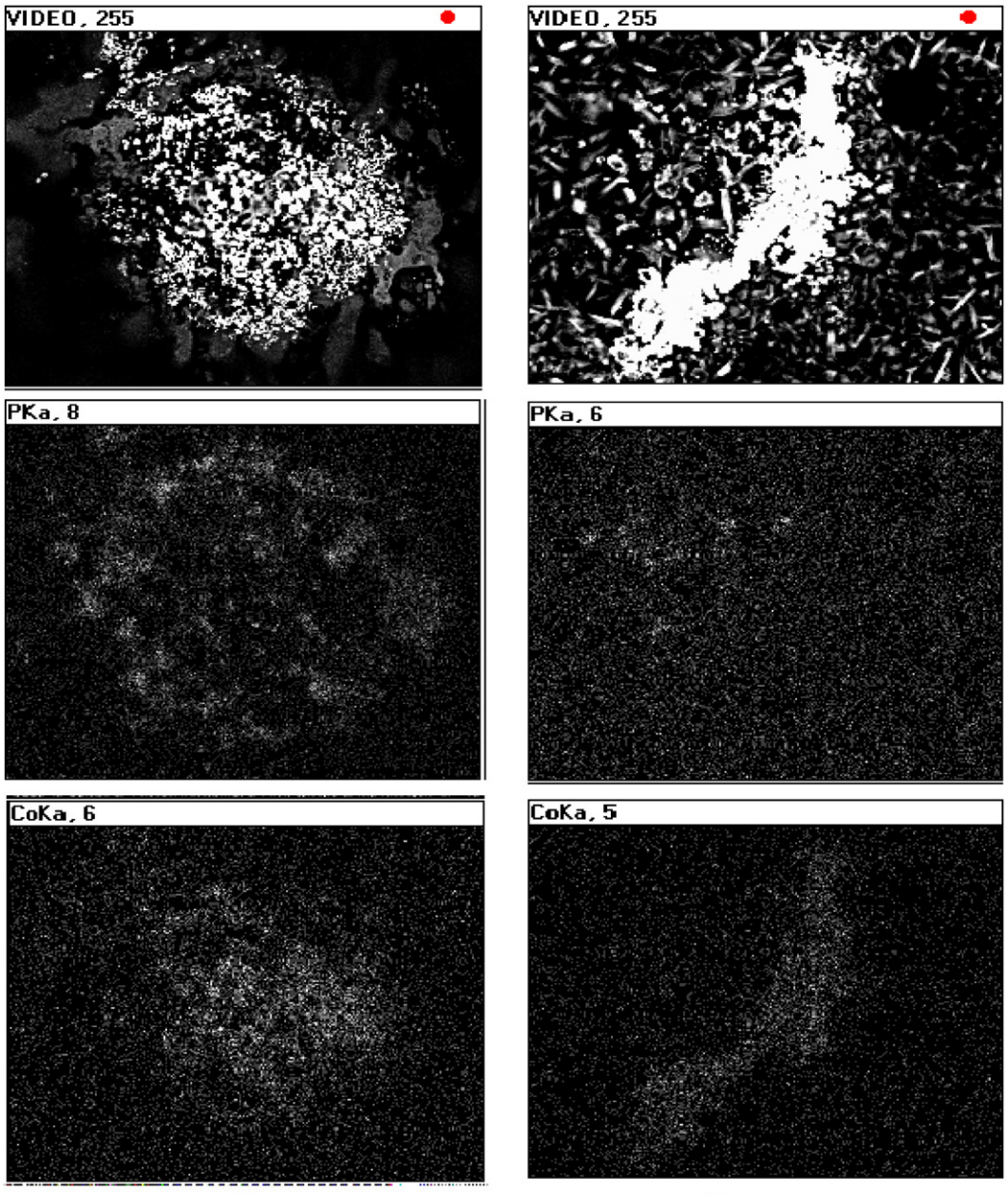

Fig. 8. EDX mapping of enamelled samples: (a) $Co_{2.3}Fe_{0.7}P_2O_{8.35}$ sample from transparent glaze and (b) $Fe_{0.5}Co_{0.5}PO_{3.75}$ sample from porcelain stoneware.

Table 3
CIE L^* a^* b^* parameters ($L^*/a^*/b^*$) in glazed tiles with addition of 5 wt.% $Co_{3-x}Fe_xP_2O_{8+x/2}$ samples fired

x	Transparent glaze[a]	Porcelain stoneware
0.00	42.63/16.09/20.31	33.10/9.82/−28.37
0.10	34.3/2.42/3.31	33.06/8.97/−27.40
0.30	33.69/0.4/−7.65	34.57/6.80/−24.74
0.50	32.83/3.55/−16.6	33.43/6.24/−23.02
0.70	33.95/7.29/−25	34.75/4.12/−21.38
1.00	34.27/5.06/−21.83	35.98/2.3/−18.57
1.50	31.35/1.71/−11.07	42.28/−1.56/-12.1
2.00	32.21/2.58/−14.01	39.26/−1.54/−10.34
Co_2SiO_4	29.0/11.2/−25.6[b]	39.7/−5.7/−9.0[b]
$Co_{0.8}Mg_{0.2}Al_2O_4$	27.5/3.3/−14.2[b]	42.1/−7.9/−22.4[b]

[a] Transparent glaze (single fire) for stoneware.
[b] From [9].

Table 4
CIE L^* a^* b^* parameters ($L^*/a^*/b^*$) in glazed tiles with addition of 5 wt.% $Fe_{1-x}Co_xPO_{4-x/2}$ samples fired

x	Transparent glaze[a]	Porcelain stoneware
0.00	29.99/9.88/−23.5	70.18/4.400/26.90
0.01	41.18/13.62/16.71	66.98/4.37/24.05
0.02	38.87/10.64/12.15	63.72/2.89/21.34
0.05	36.28/6.44/7.00	58.40/0.09/14.80
0.10	30.84/10/−25.8	57.72/−3.52/6.21
0.30	31.99/9.63/−26.3	47.56/−3.26/−7.94
0.50	31.68/9.02/−24.5	42.09/−0.80/−16.12
Co_2SiO_4	29.0/11.2/−25.6[b]	39.7/−5.7/−9.0[b]
$Co_{0.8}Mg_{0.2}Al_2O_4$	27.5/3.3/−14.2[b]	42.1/−7.9/−22.4[b]

[a] Transparent glaze (single fire) for stoneware.
[b] From [9].

4. Conclusions

$Co_3(PO_4)_2$ solid solutions and $FePO_4$ solid solutions have been obtained from $Co_{3-x}Fe_xP_2O_{8+x/2}$ ($0 \le x \le 0.30$) and $Fe_{1-x}Co_xPO_{4-x/2}$ ($0 \le x \le 0.02$) samples fired at 1000 °C. When $Co_3(PO_4)_2$ (violet) or $Co_2P_2O_7$ (blue) is detected by XRD, powdered materials are violet (blue-violet) or green ($Co_2P_2O_7$ blue and $FePO_4$ yellow). The CIE L^* a^* b^* parameters in glazed tiles with addition of samples fired at 1000 °C are different from those obtained from powdered samples.

The compositional range for which the suitable blue colour is maintained in enamelled samples is $0 \le x \le 1.0$ in $Co_{3-x}Fe_xP_2O_{8+x/2}$ compositions (between 48 and 32 wt.% Co) and it is $x \ge 0.30$ in $Fe_{1-x}Co_xPO_{4-x/2}$ compositions (about 12–20 wt.% Co). $Fe_{1-x}Co_xPO_{4-x/2}$ compositions with $0.30 \le x \le 0.50$ can be considered to minimize the Co content in blue ceramic pigments.

$Co_3(PO_4)_2$ and $Co_2P_2O_7$ structures introduce the Co^{2+} ions into glassy matrix. These structures are dissolved but ions remain in enamelled samples. The blue colour of enamelled samples is attributed to Co^{2+} ions.

Acknowledgements

We gratefully acknowledge the financial support given by MCYT, MAT 2005-00507 project.

References

[1] T.K. Ghorai, D. Dhak, A. Azizan, P. Pramanik, Investigation of phase formation temperature of nano-sized solid solution of copper/cobalt molybdate and chromium-phosphate ($M^1_xCr_{1-x}Mo_xP_{1-x}O_4$) [$M^1$ = Co, Cu], Mater. Sci. Eng. B 121 (2005) 216–223.
[2] R. El Ouenzerfi, G. Panczer, C. Goutaudier, M.T. Cohen-Adad, G. Boulon, M. Trabelsi-Ayedi, N. Kbir-Ariguib, Relationships between structural and luminescence properties in Eu^{3+}-doped oxyphosphate-silicate apatite $Ca_{2+x}La_{8-x}(SiO_4)_{6-x}(PO_4)_xO_2$, Opt. Mater. 16 (2001) 301–310.
[3] N. Clavier, N. Dacheux, P. Martinez, V. Brandel, R. Podor, P. Le Coustumer, Synthesis and characterization of low-temperature precursors of thorium-uranium (IV) phosphate-diphosphate solid solutions, J. Nuclear Mater. 335 (2004) 397–409.
[4] S.N. Achary, O.D. Jayakumar, A.K. Tyagi, S.K. Kulshresththa, Preparation, phase transition and thermal expansion studies on low-cristobalite type $Al_{1-x}Ga_xPO_4$ (x = 0.0, 0.20, 0.50, 0.80 and 1.00), J. Solid State Chem. 176 (2003) 37–46.
[5] A.A. Belik, A.P. Malakho, B.I. Lazoryak, S.S. Khasanov, Synthesis and X-ray powder diffraction study of new phosphates in the $Cu_3(PO_4)_2$-$Sr_3(PO_4)_2$ system: $Sr_{1.9}Cu_{4.1}(PO_4)_4$, $Sr_3Cu_3(PO_4)_4$, $Sr_2Cu(PO_4)_2$, and $Sr_{9.1}Cu_{1.4}(PO_4)_7$, J. Solid State Chem. 163 (2002) 121–131.
[6] DCMA, Classification and Chemical description of the Mixed Metal Oxide Inorganic Coloured Pigments, second ed., Metal Oxides and Ceramics Colors Subcommitee, Dry Color Manufacturer's Ass, Washington DC, 1982.
[7] R.K. Mason, Use of cobalt colors in glazes, Am. Ceram. Soc. Bull. 40 (1) (1961) 5–6.
[8] G. Monari, T. Manfredini, Coloring effects of synthetic inorganic cobalt pigments in fast-fired porcelainized tiles, Ceram. Eng. Sci. Process. 17 (1) (1996) 102–110.
[9] M. Llusar, A. Forés, J.A. Badenes, J. Calbo, M.A. Tena, G. Monrós, Colour analysis of some cobalt-based blue pigments, J. Eur. Ceram. Soc. 21 (2001) 1121–1130.
[10] S. Scaccia, M. Carewska, P. Wisniewski, P.P. Prosini, Morphological investigation of sub-micron $FePO_4$ and $LiFePO_4$ particles for rechargeable lithium batteries, Mater. Res. Bull. 38 (2003) 1155–1163.
[11] X. Huang, J. Ma, P. Wu, Y. Hu, J. Dai, Z. Zhu, H. Chen, H. Wang, Hydrothermal synthesis of $LiCoPO_4$ cathode materials for rechargeable lithium ion batteries, Mater. Lett. 59 (2005) 578–582.
[12] H. Onoda, K. Yokouchi, K. Kojima, H. Nariai, Addition of rare earth cation on formation and properties of various cobalt phosphates, Mater. Sci. Eng. B 116 (2005) 189–195.
[13] A.G. Nord, T. Stefanidis, Structure refinements of $Co_3(PO_4)_2$. A note on the reliability of powder diffraction studies, Acta Chemica Scandinavica A 37 (1983) 715–721.
[14] Y. Song, S. Yang, P.Y. Zavalij, M.S. Whittingham, Temperature-dependent properties of $FePO_4$ cathode materials, Mater. Res. Bull. 37 (2002) 1249–1257.
[15] Powcal and LSQC computer programmes. Department of Chemistry, Aberdeen University.
[16] Commission Internationale del'Eclairage, ''Recommendations on Uniform Color Spaces, Color Difference Equations, Phychometrics Color Terms'', Suplement n° 2 of CIE Publication N° 15 (E1-1.31) 1971 (Bureau Central de la CIE, Paris, 1978).
[17] A. Goñi, L. Lezama, A. Pujana, M.I. Arriortua, T. Rojo, Clustering of Fe^{3+} in the $Li_{1-3x}Fe_xMgPO_4$ ($0 < x < 0.1$) solid solution, Int. J. Inorg. Mater. 3 (2001) 937–942.
[18] P. Schmid-Beurmann, Syntesis and phase characterization of a solid solution series between β-$Fe_2(PO_4)O$ and $Fe_4(PO_4)_3(OH)_3$, J. Solid State Chem. 153 (2000) 237–247.
[19] A.B.P. Lever, Inorganic Electronic Spectroscopy, second ed., Elsevier Science B.V., The Netherlands, 1977, pp. 507–511.
[20] B. El Bali, M. Bolte, Refinement of cobalt diphosphate against new intensity data, Acta Crystallographica E58 (2002) i32–i33.